

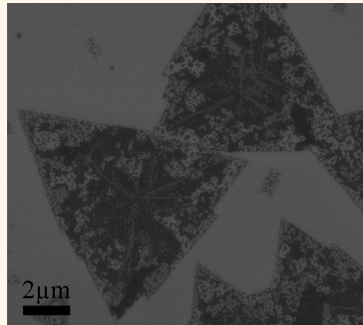
Aging of Transition Metal Dichalcogenide Monolayers

Jian Gao,[†] Baichang Li,[†] Jiawei Tan,[†] Phil Chow,[†] Toh-Ming Lu,^{*,‡} and Nikhil Koratkar^{*,†,§}

[†]Materials Science and Engineering, [‡]Physics, Applied Physics, and Astronomy, and [§]Mechanical, Aerospace and Nuclear Engineering, Rensselaer Polytechnic Institute, Troy, New York 12180, United States

 Supporting Information

ABSTRACT: Two-dimensional sheets of transition metal dichalcogenides are an emerging class of atomically thin semiconductors that are considered to be “air-stable”, similar to graphene. Here we report that, contrary to current understanding, chemical vapor deposited transition metal dichalcogenide monolayers exhibit poor long-term stability in air. After room-temperature exposure to the environment for several months, monolayers of molybdenum disulfide and tungsten disulfide undergo dramatic aging effects including extensive cracking, changes in morphology, and severe quenching of the direct gap photoluminescence. X-ray photoelectron and Auger electron spectroscopy reveal that this effect is related to gradual oxidation along the grain boundaries and the adsorption of organic contaminants. These results highlight important challenges associated with the utilization of transition metal dichalcogenide monolayers in electronic and optoelectronic devices. We also demonstrate a potential solution to this problem, featuring encapsulation of the monolayer sheet by a 10–20 nm thick optically transparent polymer (parylene C). This strategy is shown to successfully prevent the degradation of the monolayer material under accelerated aging (*i.e.*, high-temperature, oxygen-rich) conditions.



KEYWORDS: transition metal dichalcogenides, aging, environmental degradation, oxidation, polymer encapsulation

The lack of a band gap in graphene has spurred intense interest in two-dimensional semiconducting transition metal dichalcogenides (TMDs). These materials have the stoichiometric formula MX_2 , with a trigonal prismatic structure comprised of atomic layers of chalcogens (X = S, Se) and group VI transition metals (M = Mo, W).^{1,2} They can be produced in bulk form but also as few-layered as well as monolayer sheets. It is well understood that a monolayer of trigonal prismatic semiconducting TMDs exhibits a direct band gap (in the range 1.5–2 eV) that it is not present in few-layered systems. This direct band gap is what differentiates monolayer TMDs from other 2D materials such as graphene, which is a zero band gap semimetal. Semiconductor TMDs exhibit remarkably enhanced interaction^{3–5} with visible light due to this indirect-to-direct band gap conversion at the monolayer limit, rendering these systems versatile platforms for studying light–matter interactions and for optoelectronic device applications.

Unlike the fast degradation of black phosphorus in air,^{6–8} TMDs have been considered as air-stable semiconductors under ambient conditions.^{9,10} While there are some reports that show degradation of TMDs under extreme conditions¹¹ such as temperatures above 250 °C and combined exposure to UV, heat, and moisture,^{12,13} there is no prior report showing significant degradation of monolayer TMDs under ambient conditions (room temperature and atmospheric pressure). Prior efforts at shielding TMDs from the environment have

been primarily motivated by the need to prevent molecular adsorbates and charge traps from affecting the carrier mobility of TMDs. In one approach,¹⁰ hexagonal boron nitride (h-BN) was used as the encapsulation layer for exfoliated MoS₂, but the stacking of large-scale exfoliated h-BN may not be practical, and there are inevitable voids and cracks in chemical vapor deposition grown and transferred^{14,15} h-BN. Encapsulation by continuous metal oxide layers, deposited by atomic layer deposition (ALD), represents another strategy,¹⁶ but this method is not well suited for flexible electronics due to crack propagation² under strain. Polymer-based encapsulation methods, however, are not limited by such restrictions^{17,18} and could offer an effective approach to shield TMD materials from the environment.

In this work, we investigated the long-time (6–12 months) stability of monolayer semiconducting TMDs such as MoS₂ and WS₂ in air under ambient conditions (*i.e.*, room temperature and atmospheric pressure). Using scanning electron microscopy (SEM), spatially resolved photoluminescence (PL) measurements, and X-ray photoelectron spectroscopy (XPS), we demonstrate the susceptibility of TMD monolayers to ambient degradation. In fact, we report large-scale structural and morphological changes to the sheets and intense

Received: December 6, 2015

Accepted: January 25, 2016

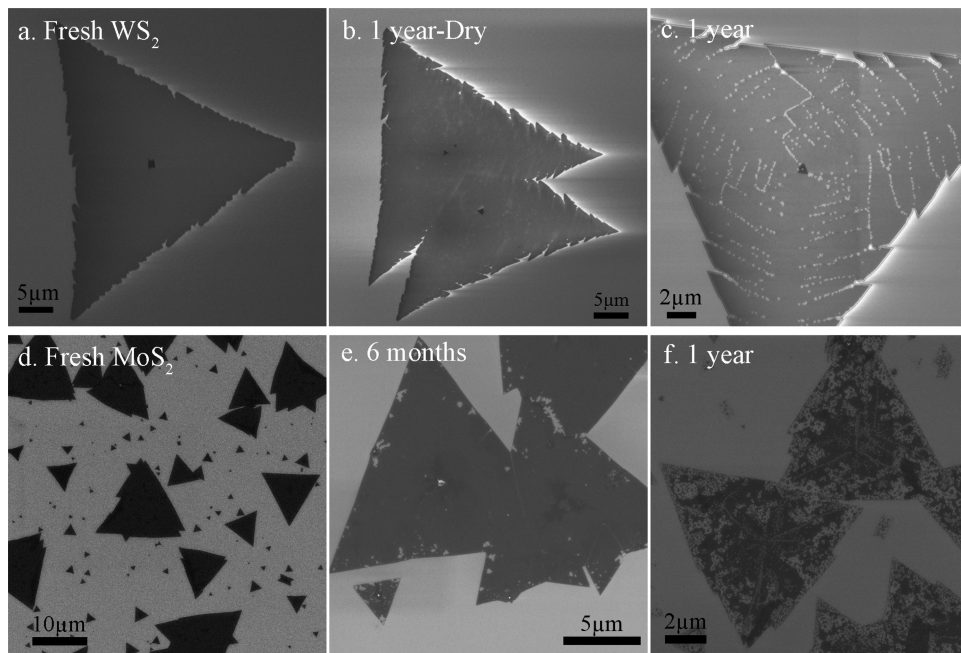


Figure 1. Scanning electron microscopy (SEM) images of (a) fresh WS_2 , aged WS_2 after 1 year in a container (b) with and (c) without desiccant, (d) fresh MoS_2 , and (e) aged MoS_2 after 6 months without desiccant and (f) after 1 year without desiccant. All the samples were stored in Class 100 cleanroom conditions.

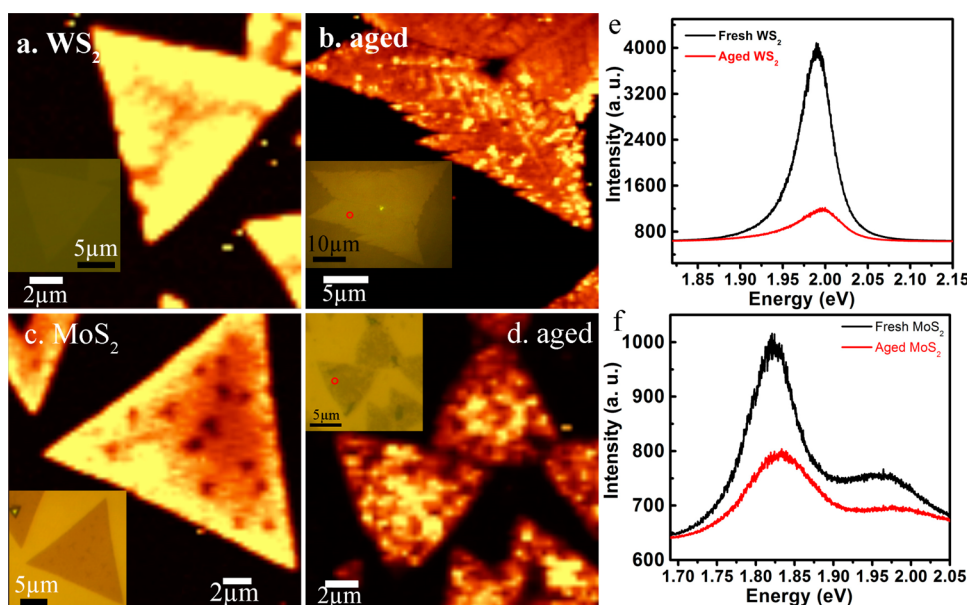


Figure 2. Photoluminescence spectra of fresh and aged TMDs. PL intensity map (centered at the A exciton) of fresh WS_2 (a), WS_2 aged for 1 year under ambient conditions (b), fresh MoS_2 (c), and MoS_2 aged for 1 year under ambient conditions (d). The inset optical images show the WS_2 and MoS_2 flakes from which the data were taken. (e, f) Representative PL spectra of the fresh and 1-year-aged WS_2 (e) and fresh and 1-year-aged MoS_2 (f). Both the monolayer WS_2 and MoS_2 films were aged for 1 year under ambient conditions (*i.e.*, room temperature and atmospheric pressure).

degradation in the optical behavior. This indicates that the generally accepted view that monolayer TMDs are air-stable materials under ambient conditions is incorrect and needs to be revised. Our results indicate adsorption of organic materials from the ambient and the gradual oxidation of TMDs along grain boundaries over a period of months. Finally, we report a possible solution to this problem by encapsulation of TMD sheets with optically transparent and ultrathin (10–20 nm) polymeric films (*e.g.*, parylene C). Such a polymer encapsula-

tion strategy could protect monolayer TMDs and pave the way for the realization of air-stable and high-performance TMD-based electronic and optoelectronic devices.^{19,20}

RESULTS AND DISCUSSION

Monolayer WS_2 on sapphire and monolayer MoS_2 on 300 nm SiO_2/Si were synthesized using chemical vapor deposition ([Materials and Methods](#)) with grain size of tens of micrometers, as shown in Figure 1a and d. The surface is uniform and

continuous, with only some small multilayer regions. However, after being stored at room temperature ($\sim 25^\circ\text{C}$) in a container with desiccant for 1 year (Figure 1b), cracks formed in all the WS_2 sheets, especially along the grain boundaries. WS_2 monolayers that were exposed to moisture-rich conditions (*i.e.*, without drying desiccant) at room temperature went through even more severe structural and morphological changes over the 1-year period, as shown in Figure 1c (almost the entire WS_2 sheet exhibits visible degradation). Figure 1b and c indicate that high-humidity conditions severely accelerate the degradation of WS_2 . Additionally, we find that chemical vapor deposited MoS_2 also went through similar gradual deterioration, with the grain boundaries and edges first being oxidized in 6 months and almost the whole crystal in 1 year (Figure 1d–f). The oxidation and aging of the MoS_2 sheets were also confirmed by testing transistor devices (Supplementary Figure S1) in the fresh and aged state. We find that the device current decreased almost 2 orders of magnitude after 1 month, indicating damage due to the aging. In addition, the threshold voltage increased from -16 V to -9 V , which is consistent with p-type doping induced by oxidation of the MoS_2 sheet. Note that the images in Figure 1 are typical of chemical vapor deposition (CVD)-grown TMD films, and we have verified this by imaging flakes at different locations on the substrate. The gradual deterioration of the samples over a period of months was consistent in all of the CVD-grown TMD films that we have imaged.

We characterized the fresh and aged (1 year) CVD-grown WS_2 and MoS_2 monolayer sheets by room-temperature PL measurements using a WITec alpha300R spectrometer equipped with a 532 nm excitation laser and Si-based CCD detector. The integrated PL intensity map of a typical fresh WS_2 sheet is shown in Figure 2a (the optical image of the flake is shown in the inset image). Figure 2b shows the corresponding PL mapping and the optical image (inset) of typical 1-year-old WS_2 sheets. It is clear that there is significant spatial variation in the PL intensities in Figure 2b, with certain regions exhibiting severe PL quenching indicative of extensive damage to the samples. To further analyze the PL signature, we carried out curve fitting of the PL spectra (Supplementary Figure S2) for the 1-year-aged monolayer WS_2 and compared the results to freshly grown WS_2 . The optimal line shape for the spectral contributions is a mixed Gaussian–Lorentzian function as shown in our previous work.⁵ In the PL spectra of both fresh and aged WS_2 , a lower-energy tail associated with the A-exciton peak is observed, attributed to the trion emission, resulting from residual charge doping^{21,22} or from charged impurities.^{23,24} The B-exciton peak is not present in the spectra of WS_2 due to the PL photodetector range, but a distinct shoulder at around 1.9 eV is observed in only the aged WS_2 , which has been attributed in the literature to defects.⁵ One important observation from the measured PL spectra (Figure 2e) is that the PL intensity of the 1-year-aged WS_2 sample is ~ 6 times lower as compared to the fresh WS_2 , which indicates severe PL quenching due to the oxidation of the WS_2 sheet. The PL for the 1-year-old WS_2 is also significantly broadened (Supplementary Figure S2) as compared to the fresh sample. The measured full widths at half-maximum (fwhm) of the A-exciton, trion, and defect PL peaks are $\sim 0.050\text{ eV}$ ($\sim 0.036\text{ eV}$), $\sim 0.059\text{ eV}$ ($\sim 0.046\text{ eV}$), and $\sim 0.088\text{ eV}$ ($\sim 0.045\text{ eV}$) for the 1-year-old WS_2 (fresh WS_2) samples. The PL contribution⁵ from defects (X^D) increased from $\sim 1.5\%$ (of the A-exciton intensity) for the

fresh WS_2 to $\sim 18.7\%$ for the aged sample, which indicates significant deterioration of the aged sample.

Figure 2c shows PL mapping and the optical image (inset) of a typical freshly grown MoS_2 sheet, while Figure 2d shows the PL mapping of a typical 1-year-old MoS_2 sample showing significant PL quenching and spatial variation in the PL intensity. The PL spectrum (Figure 2f) of MoS_2 is mainly dominated by neutral A-exciton emission, along with B-exciton emission arising from the spin–orbital splitting of the valence band, $\sim 150\text{ meV}$ away from the A peak.^{23,25–28} We observed a significant broadening of the A and B excitons and trion peaks for the 1-year-aged MoS_2 (Supplementary Figure S2) as compared to the fresh sample. The fwhm's of A-exciton, B-exciton, and trion peaks are $\sim 0.090\text{ eV}$ ($\sim 0.061\text{ eV}$), $\sim 0.202\text{ eV}$ ($\sim 0.161\text{ eV}$), and $\sim 0.091\text{ eV}$ ($\sim 0.065\text{ eV}$) for the 1-year-old MoS_2 (fresh MoS_2). Similar to the WS_2 case, we observe severe PL quenching for the 1-year-old MoS_2 sample; the PL intensity of the 1-year-aged MoS_2 sample was measured to be ~ 2.3 times lower (Figure 2f) as compared to the fresh MoS_2 . Note that the PL spectra in Figure 2e,f are taken from different flakes on the same film. This was because over a period of 1 year we were unable to pinpoint and monitor the exact same flake. However, for statistics we checked multiple points on different flakes, and we find that the overall PL intensity decreased by 2- to 6-fold for the aged samples when compared to the pristine or fresh ones.

To study the chemical nature of the aging process, we have utilized room-temperature XPS, comparing fresh and 1-year-aged samples in Figure 3. Data for 6-month-aged samples

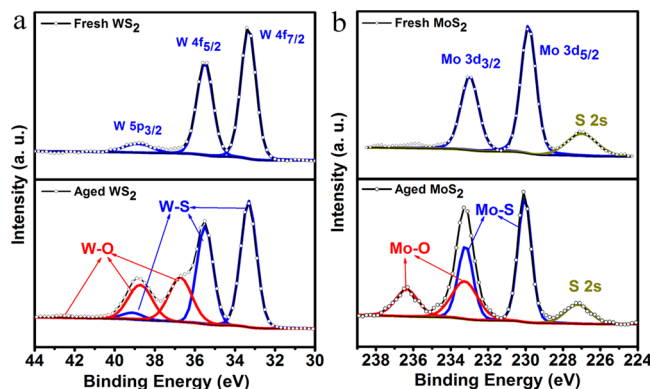


Figure 3. XPS spectra (calibrated using the adventitious carbon C 1s peak) of fresh and 1-year-aged WS_2 (a) and fresh and 1-year-aged MoS_2 (b) showing W 4f (a), Mo 3d (b), with Gaussian–Lorentzian fitting of each peak. The W 4f (Mo 3d) contributions exhibit two distinct sets of peaks after 1 year.

(Supplementary Figure S3) show similar trends. In fresh WS_2 , the W:S ratio is $\sim 1:2$, with only one chemical state doublet in the W 4f core-level spectra (with $\text{W } 4f_{7/2}$ at 33.4 eV and $\text{W } 4f_{5/2}$ at 35.5 eV). However, the W:S ratio after one year is reduced to 1:1.33 in the aged WS_2 , indicating intense sulfur loss (Figure 3a). Furthermore, the W 4f core-level spectra recorded from the aged WS_2 samples show an additional doublet feature at higher binding energies ($\sim 3.1\text{ eV}$), indicating the presence of tungsten in a higher oxidation state²⁹ than pristine WS_2 . The three new peaks (red curves) with higher binding energy originate from the oxidized W ($\text{W}-\text{O}$), and the remaining three peaks (blue curves) are corresponding to the S-bound W ($\text{W}-\text{S}$). It should be noted that the sulfur is still bound

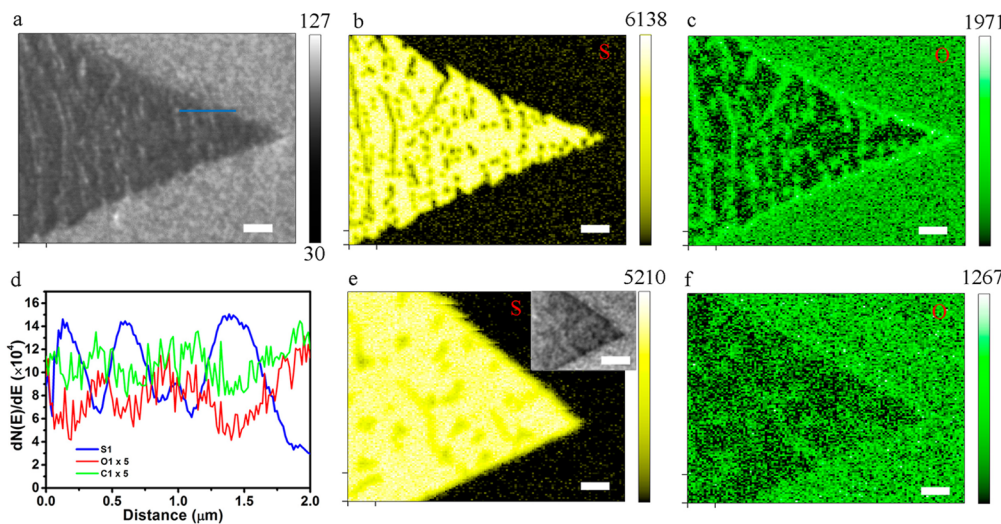


Figure 4. (a) SEM image of the aged WS_2 on Au substrate, taken in an Phi 700 scanning Auger nanoprobe. (b, c) AES mapping images for S and O of 1-year-aged WS_2 . (d) Auger electron spectroscopy (AES) line profile of the line marked in (a). (e, f) AES mapping images for S and O of fresh WS_2 . Inset: SEM image of the fresh WS_2 (scale bar: 1 μm).

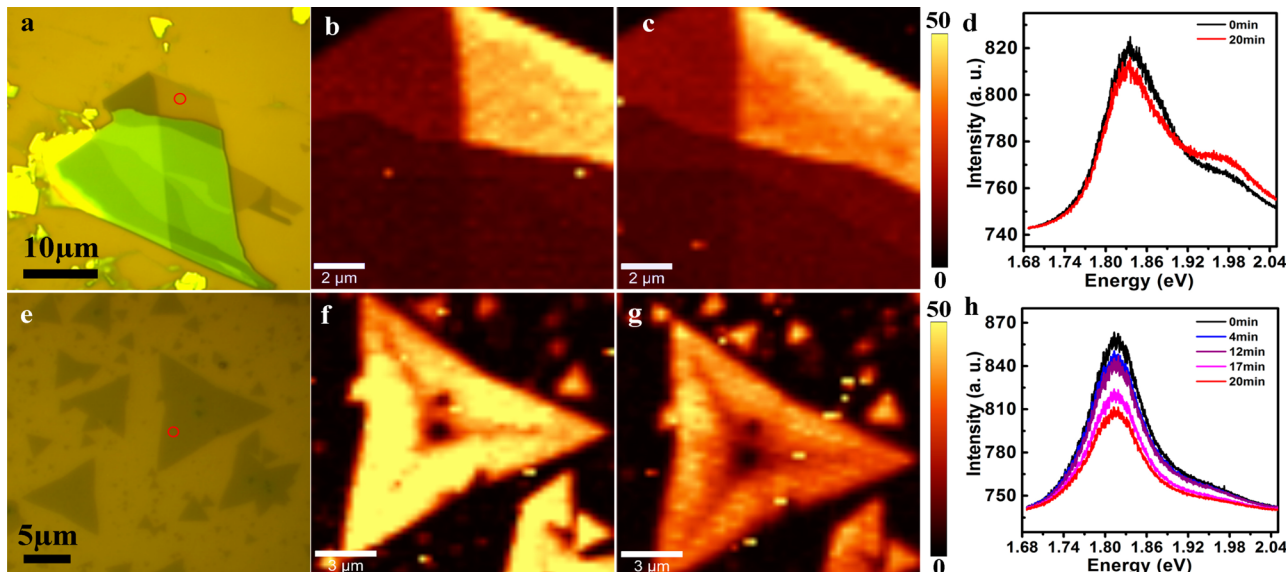


Figure 5. (a) Exfoliated MoS_2 flake on SiO_2/Si substrate. (b) PL mapping of MoS_2 flake prior to the accelerated aging test. Only the monolayer region shows high PL intensity. (c) PL map of the same MoS_2 flake after accelerated aging for ~20 min at ~80 °C and a humidity of ~65%. (d) Typical PL spectra of the monolayer region before (black) and after (red) the accelerated aging treatment. (e) CVD-grown monolayer MoS_2 on SiO_2/Si substrate. (f) PL map of a CVD-grown MoS_2 sheet prior to accelerated aging. (g) PL map of the same sheet after ~20 min of accelerated aging at ~80 °C and a humidity of ~65%. (h) Change in the PL spectra of the CVD-grown MoS_2 sheet during the accelerated aging test. Note that the red circle in (a) and (c) marks the spot where the PL spectrum was taken.

exclusively to W without exhibiting any extra chemical states, as shown in the [Supplementary Figure S4](#).

XPS analysis for the MoS_2 ([Figure 3b](#)) indicates that the Mo:S ratio decreases from ~1:2 in the fresh sample to ~1:1.05 in the aged MoS_2 , and an extra Mo 3d chemical state doublet appears with binding energies that are ~3.3 eV higher than Mo–S 3d. The percentage of oxidized Mo (Mo–O) (red curves) is ~34.8% for the 1-year-aged MoS_2 . For comparison, a 6-month-aged monolayer MoS_2 sample was also characterized by XPS ([Supplementary Figure S3](#)). The calculated percentage of the Mo–O state was ~14.4% for the 6-month-aged sample compared to ~34.8% for the 1-year-old sample, confirming progressive oxidation over time. Furthermore, only one peak (at 533.1 eV) fits (see [Supplementary Figure S5](#)) with the O 1s

core-level spectra for the fresh MoS_2 , which is corresponding to the O 1s state from the SiO_2 substrate and is unrelated to the MoS_2 sheet. However, two more O 1s singlet peaks are needed ([Supplementary Figure S5](#)) to fit the aged MoS_2 sample, with the one at 531.4 eV matching the organic C–O binding energy for O 1s, while the other one at 530.5 eV corresponds to the metal oxide state.^{30,31} This result suggests that, in addition to the “oxidation” of the transition metal, oxygen is also present in the aged sample in the form of “organic contaminants” that are adsorbed onto the aged sheets. The XPS analysis did not indicate the formation of any sulfur oxide (SO_x) under ambient conditions for the aged TMD samples, which indicates that S atoms are being displaced by oxygen in these films. The mechanism for the S loss is not clear at this point and will

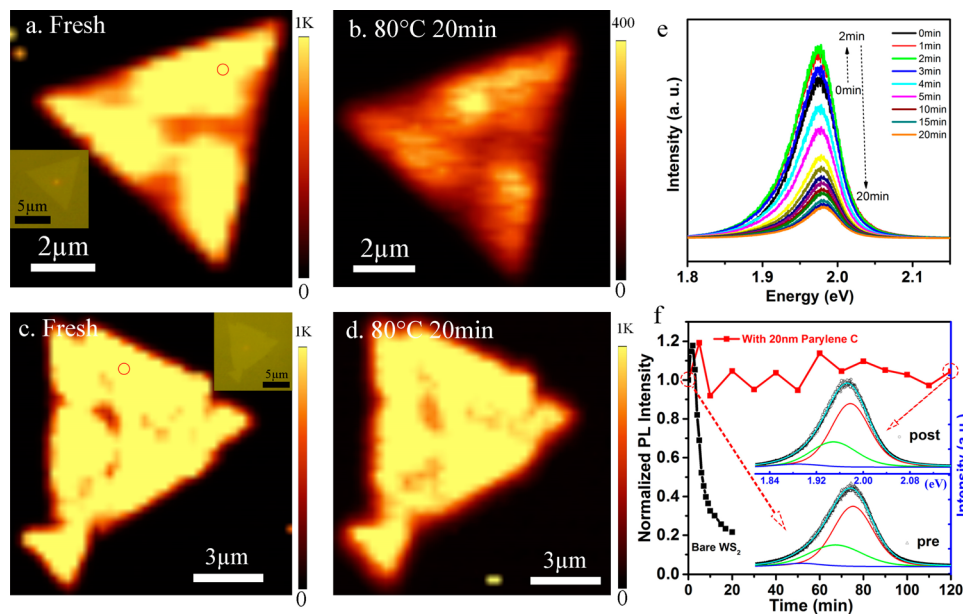


Figure 6. Integrated PL intensity map of fresh WS₂ and WS₂ subjected to accelerated aging at $\sim 80^{\circ}\text{C}$ and $\sim 65\%$ humidity. (a, b) Bare WS₂ without parylene C coating. (c, d) WS₂ with ~ 20 nm parylene C coating. (e) Time dependence of PL spectra of bare WS₂ during the accelerated aging test. (f) Time dependence of the PL intensity of WS₂ (normalized to the PL intensity prior to the accelerated aging test) *vs* the oxidation time. Black: Bare WS₂; red: WS₂ with 20 nm parylene C coating. Insets: PL spectra of WS₂ coated with parylene C (bottom: before the accelerated aging; top: after ~ 120 min of accelerated aging). Note that the red circle in (a) and (c) marks the spot where the PL spectrum was taken.

require additional study. One possibility is that O is first bonded to S, followed by breaking of the S–metal bond, followed by substitution of the S by O or OH radicals. Such processes are likely initiated or catalyzed at regions with S deficiency (such as defects and grain boundaries) and then gradually propagated throughout the entire TMD sheet.

XPS analysis (Figure 3) has shown the nature of gradual oxidation of the TMDs over time. In addition, we performed Auger electron spectroscopy (AES) to probe the chemical distribution of the aged WS₂ by transferring it onto a ~ 50 nm thick Au substrate. Note that the WS₂ sheet was aged for the 1-year period on sapphire and was transferred to the Au surface only for the purpose of the Auger study. A scan over the line marked in Figure 4a indicates the opposing distributions (Figure 4d) of S and O (or C). The sulfur content varies periodically, dipping in the proximity of the grain boundaries and rising in the center of the grains. The increase (decrease) in S content is matched (Figure 4d) in the line scan by a corresponding decrease (increase) in the O and C content, which indicates extensive oxidation and adsorption of organic materials at the grain boundaries. These conclusions are also confirmed by the high spatial resolution AES elemental mapping results shown in Figure 4b,c for the aged WS₂ sheet. The oxygen concentration is markedly greater (Figure 4c) along the grain boundaries and edges of the aged WS₂ sheet. The corresponding sulfur concentration (Figure 4b) is very low or even totally depleted in these regions. Carbon was also detected (Supplementary Figure S6), especially at the oxidized regions, indicating the preferred adsorption of organic species and hydrocarbons at the oxidized regions of the WS₂ sheets. For comparison, a freshly grown (*i.e.*, non-aged) WS₂ sheet transferred on the Au substrate was also characterized (Figure 4e,f) as a control. The sulfur distribution of the fresh WS₂ (Figure 4e) is far more uniform than that of the aged WS₂, while the relative oxygen intensity (Figure 4f) was also lower

than that in the aged WS₂. From the XPS and AES characterizations (Figures 3 and 4), along with the SEM images (Figure 1), we conclude that the monolayer TMD sheets undergo gradual oxidation, which is initiated from the crystal edges, grain boundaries, and defects, and then propagates over time into the TMD grains. This results in significant structural changes, cracking, and PL quenching of the TMD sheets over a period of months. Besides oxidation, we see evidence of adsorption of organic molecules on TMD surfaces over time, which has also been reported^{32,33} in wettability studies of TMDs.

In order to better understand the aging mechanism, we carried out accelerated aging tests (at high temperature and under humid conditions) on mechanically exfoliated (using adhesive tape) monolayer MoS₂ on a SiO₂/Si substrate and CVD-grown monolayer MoS₂ on a SiO₂/Si substrate. The results (Figure 5) indicate that aging of exfoliated MoS₂ is very different when compared to CVD-grown MoS₂ under the exact same conditions (~ 20 min at $\sim 80^{\circ}\text{C}$ and a humidity of $\sim 65\%$). While the CVD-grown sample exhibits large PL quenching, the monocrystalline exfoliated sample shows only a slight reduction in the PL intensity. This suggests that the presence of S vacancies (substoichiometry) along the grain boundaries in CVD-grown samples plays a crucial role. It has been shown that chalcogen vacancies are thermodynamically favorable to be replaced with substitutional oxygen atoms,⁴ and therefore, S vacancies at the grain boundaries in polycrystalline samples could greatly accelerate the oxidation process in CVD samples as compared to the monocrystalline exfoliated ones.

It is clear from our results that oxidation occurs at the edges and grain boundaries of the CVD-grown TMD sheets. Further, the comparison of accelerated aging of CVD and mechanically exfoliated samples on the same substrate indicates that monocrystalline (exfoliated) samples are more resistant to aging than polycrystalline CVD-grown ones (Figure 5). We also

find that exposure to humidity and temperature significantly accelerates the aging process. On the basis of these observations, we propose the following hypothesis for the aging process. It appears that the oxidation is initiated due to substoichiometry at defects, grain boundaries, and edges in the TMD sheets. While XPS analysis indicates W:S and Mo:S ratios in CVD-grown samples as ~1:2, this is an average over the entire sample and does not capture “local substoichiometries” that are likely to exist along the grain boundaries, sheet edges, and defects in the TMD sheets. It has been shown that chalcogen vacancies are thermodynamically favorable to be replaced with substitutional oxygen atoms,^{4,34,35} and therefore we expect that O and OH radicals will be attached to the grain boundaries and sheet edges. Once the oxidation process is initiated, it then gradually penetrates into the TMD grains as more and more of the S atoms are replaced by O, and this process becomes more energetically favorable as the ambient humidity and temperature are raised. While the above hypothesis offers a reasonable explanation for our observations, our expectation is that this study will spur more in-depth modeling and simulation work of oxidation and corrosion in monolayer TMD materials.

To protect TMDs from environmental attack, we explored the possibility of encapsulating the TMD sheet with ultrathin and minimally invasive polymer layers. As moisture and oxygen are crucial in the TMD degradation process, we chose parylene C as the encapsulation layer due to its low water and oxygen permeability (*Supporting Information*). To evaluate the effectiveness of parylene C as a protective barrier coating, we performed an accelerated aging test at elevated temperature and under humid conditions. First, we carried out accelerated aging of the bare WS₂ without the parylene C coating as a control. After oxidation at ~80 °C and ~65% humidity for ~20 min (*Figure 6b*), the PL intensity exhibited a dramatic (~5-fold) decrease across the entire crystal when compared to the PL intensity (*Figure 6a*) of the same WS₂ sheet prior to the accelerated aging test. *Figure 6e* shows the PL quenching of the unprotected WS₂ sheet over the 20 min duration of the accelerated aging test. For these tests, the PL spectroscopy stage was maintained at ~80 °C (humidity at ~65%), and the data were acquired *in situ* (with the laser turned off between each measurement). Note that the intensity of the PL increased slightly during the first 2 min, which is presumably caused by a reduction in n-doping, due to electron transfer from WS₂ to adsorbed water. However, subsequently the PL intensity decreases sharply during the accelerated aging test. The PL peak is also slightly blue-shifted due to enhanced p-doping induced by the oxidation. The Lorentzian–Gaussian fitted PL spectra after 0 and 20 min of the accelerated aging treatment are shown in *Supplementary Figure S7*, with the defect peak (X^D) contribution³ increasing from ~5.7% to ~14.9%, which confirms that the bare (*i.e.*, unprotected) WS₂ is significantly degraded during the accelerated aging test. To compare the damage induced by accelerated aging *vs* ambient aging, we imaged the exact same region of WS₂ on sapphire (*Supplementary Figure S8*) before and after accelerated oxidation for ~20 min at ~80 °C and a humidity of ~65%. The imaging of the same region after accelerated aging shows the appearance of cracks, as is typical of ambient aging (*Figure 1*).

Next, a thin layer (~20 nm) of parylene C was deposited (*Materials and Methods*) on a freshly grown monolayer WS₂ sheet. Note that parylene C is optically transparent, and we do

not observe any significant alteration to the PL and Raman signatures of WS₂ for parylene C coatings of 2–20 nm as shown in *Supplementary Figure S9*. The parylene-coated WS₂ sheets were subjected to accelerated aging for ~20 min under the same conditions as the control (*i.e.*, unprotected WS₂) samples. Comparing the PL intensity maps of before (*Figure 6c*) and after (*Figure 6d*) the accelerated aging test, it is clear that the ~20 nm thick parylene C has fully protected the WS₂ from the fast oxidation, without any noticeable PL intensity change across the whole crystal. We then proceeded to continue the accelerated aging test for the parylene-protected WS₂ sheet from ~20 min up to ~120 min. As summarized in *Figure 6f*, the PL intensity of 20 nm parylene C coated WS₂ showed no significant change over 120 min, while the PL intensity of the bare (unprotected) WS₂ drastically decreased in less than 20 min of accelerated aging. The PL line shapes of WS₂ with ~20 nm parylene C before and after the accelerated aging test are shown in the inset of *Figure 6f*, indicating no significant differences in the neutral, trion, and defect signatures. The accelerated aging tests shown in *Figure 6* indicate that a 10–20 nm thick parylene C coating could be sufficient to protect the TMD from environmental attack; however long-term testing over several months to years under ambient conditions is needed to establish this.

In addition to parylene C, we also studied the protection ability of poly(methyl methacrylate) (PMMA, molecular weight of 950k) coatings. For this test, a MoS₂ sheet was coated with ~200 nm thick PMMA film. This PMMA-protected sample was placed together with the unprotected MoS₂ samples shown previously in *Figure 1d*. Comparing the SEM images of unprotected MoS₂ (*Figure 1d*) and protected MoS₂ (*Supplementary Figure S10*) after aging for 1 year, it is evident that the MoS₂ was greatly protected by PMMA encapsulation, with only the edges attacked. The XPS spectrum of PMMA-coated MoS₂ (*Supplementary Figure S11*) was taken after dissolving and removing PMMA in acetone overnight. Surprisingly, only a small amount of the oxidized Mo was detected, with a Mo:S ratio of ~1:1.96. While it is clear that the PMMA film has performed adequately in protecting monolayer MoS₂ over the 1-year period, we expect the parylene C to perform even better. The reason is that PMMA can absorb as high as ~2% w/w water,³⁶ and the permeability to water of PMMA is ~6 orders of magnitude higher³⁷ than that of parylene C. As oxidation is sensitive to moisture, we expect superior protection from parylene C films as compared to PMMA. Future work should focus on comparing various polymer encapsulation treatments as well as optimizing the polymer capping layer thickness for the successful long-term protection of monolayer TMD films. There are of course situations where polymer encapsulation may not be suitable; for example, for processing reasons or in high-temperature applications. In such situations alternative encapsulation methods^{10,16} such as carbon coatings or atomic layer deposition methods, should be investigated.

CONCLUSION

To conclude, we have shown that chemical vapor deposited monolayer TMD materials are not air stable under ambient conditions (room temperature and atmospheric pressure) and are prone to environmental degradation over a period of several months. The gradual oxidation of these atomically thin materials in ambient conditions occurs due to the presence of oxygen and moisture. In fact, within 1 year, the monolayer MoS₂ and WS₂ sheets became noncontinuous and the PL

emission drastically decreased. Chemical analysis by X-ray photoelectron and Auger electron spectroscopy indicates the presence of oxidized metal states, along with organic adsorbates. We also show that capping TMD sheets with polymeric films (such as parylene and poly(methyl methacrylate)) has the potential to suppress the aging and deterioration of monolayer TMD materials, which could facilitate the development of “air-stable” electronic and optoelectronic devices using these materials.

Future work should investigate the air-stability of TMDs with chalcogens other than S, as well as careful optimization of the capping or encapsulation layer for prolonged stability under ambient conditions. Another factor that needs to be studied in detail is the role of the substrate. For example, substrates that give better epitaxy for TMDs could render them more robust against ambient attack. The wettability of the substrate could also play an important role. For example, substrates that are significantly more hydrophobic than SiO_2/Si could be far more resistant to environmental attack under wet and humid conditions. Most importantly, in-depth modeling and simulation work of corrosion in monolayer TMD materials to understand the mechanism(s) by which sulfur is lost and replaced by oxygen is necessary.

MATERIALS AND METHODS

Materials Preparation. Sapphire substrates were loaded into the CVD furnace and placed above an alumina boat with 200 mg of WO_3 (Alfa Aesar #013398). A boat with 200 mg of sulfur (Alfa Aesar #010755-18) was located upstream wrapped with a heating belt. When the furnace temperature reached $\sim 900\text{ }^\circ\text{C}$ at a ramping rate of $\sim 18\text{ }^\circ\text{C}/\text{min}$, the heating belt temperature was raised to $\sim 100\text{ }^\circ\text{C}$. The CVD growth was performed at $\sim 120\text{ mTorr}$ for $\sim 30\text{ min}$ while flowing ultra-high-purity argon gas at $\sim 80\text{ sccm}$ (mixed with $\sim 3\%$ H_2). After the reaction, the furnace lid was opened to naturally cool the furnace to $\sim 200\text{ }^\circ\text{C}$. MoS_2 was grown on a 300 nm SiO_2/Si wafer in a 2 in. CVD furnace, with 20 mg of MoO_3 and 200 mg of sulfur (Alfa Aesar #010755-18). The furnace temperature was ramped to $\sim 700\text{ }^\circ\text{C}$ at a rate of $\sim 18\text{ }^\circ\text{C}/\text{min}$, then kept at $\sim 700\text{ }^\circ\text{C}$ for $\sim 10\text{ min}$, while flowing ultra-high-purity nitrogen gas at $\sim 50\text{ sccm}$. The parylene C was deposited by a Union Carbide parylene coater, and the thickness was measured by ellipsometry.

Characterization. Raman and PL spectroscopy were performed using a WITec alpha300R spectrometer equipped with a 532 nm excited line and CCD detector in a backscattering geometry and a heating stage. All PL spectra are collected for the same laser power ($\sim 1\text{ mW}$) and the same integration time ($\sim 0.5\text{ s}$). The PL mapping was conducted by a moving step of $\sim 0.3\text{ }\mu\text{m}$ and integration time of $\sim 0.1\text{ s}$, at a laser intensity of $\sim 1\text{ mW}$. The energies of the PL maps are centered at the A-exciton peak for both WS_2 and MoS_2 . All measurements were carried out in air at $\sim 25\text{ }^\circ\text{C}$ and atmosphere pressure, except the accelerated aging measurements, which were conducted at $\sim 80\text{ }^\circ\text{C}$ and a humidity of $\sim 65\%$. The XPS was performed using a PHI 5400 X-ray photoelectron spectrometer equipped with a monochromatic Al $\text{K}\alpha$ source ($\lambda = 1486.7\text{ eV}$). The detector pass energy was set to 23.5 eV, and the sample surface-to-detector takeoff angle was set at 45° . The 284.8 eV adventitious C 1s peak was used for charging corrections because it was detectable for both $\text{WS}_2/\text{sapphire}$ and $\text{MoS}_2/\text{SiO}_2$. The XPS data fitting was conducted in PHI MultiPak. Auger electron spectra were taken by a PHI 700 scanning Auger nanoprobe operating at 10 kV and 10 nA.

ASSOCIATED CONTENT

Supporting Information

The Supporting Information is available free of charge on the ACS Publications website at DOI: [10.1021/acsnano.5b07677](https://doi.org/10.1021/acsnano.5b07677).

Details regarding properties of polymer films used for TMD encapsulation and stoichiometric calculations for XPS, electrical testing of transistor devices in the fresh and aged states, Gaussian–Lorentzian fitting of the PL spectra of fresh and aged TMD samples, XPS characterization of 6-month-aged samples, XPS spectra of the core-level binding energies of S 2p for fresh and 12-month-aged MoS_2 and WS_2 sheets, O 1s core-level spectra results for fresh and aged TMD samples, AES mapping for carbon and tungsten of fresh and aged WS_2 sheets, PL spectra of bare WS_2 before and after 20 min of oxidation treatment, imaging of WS_2 on sapphire before and after an accelerated aging test, Raman spectra of WS_2 with and without parylene C coating, SEM images of MoS_2 protected by PMMA coating (after 1 year in air), and XPS spectra of PMMA-protected MoS_2 samples (PDF)

AUTHOR INFORMATION

Corresponding Authors

*E-mail (T.-M. Lu): lut@rpi.edu.

*E-mail (N. Koratkar): koratn@rpi.edu.

Notes

The authors declare no competing financial interest.

ACKNOWLEDGMENTS

N.K. and T.M.L. acknowledge funding support from the USA National Science Foundation (Award Numbers 1234641, 1435783, and 1510828), New York State under NYSTAR program C080117, and the John A. Clark and Edward T. Crossan Endowed Chair Professorship at the Rensselaer Polytechnic Institute.

REFERENCES

- (1) Kim, I. S.; Sangwan, V. K.; Jariwala, D.; Wood, J. D.; Park, S.; Chen, K.-S.; Shi, F.; Ruiz-Zepeda, F.; Ponce, A.; Jose-Yacaman, M.; Dravid, V. P.; Marks, T. J.; Hersam, M. C.; Lauhon, L. J. Influence of Stoichiometry on the Optical and Electrical Properties of Chemical Vapor Deposition Derived MoS_2 . *ACS Nano* **2014**, *8*, 10551–10558.
- (2) Chang, H. Y.; Yang, S.; Lee, J.; Tao, L.; Hwang, W. S.; Jena, D.; Lu, N.; Akinwande, D. High-Performance, Highly Bendable MoS_2 Transistors with High-K Dielectrics for Flexible Low-Power Systems. *ACS Nano* **2013**, *7*, 5446–5452.
- (3) Sangwan, V. K.; Jariwala, D.; Kim, I. S.; Chen, K. S.; Marks, T. J.; Lauhon, L. J.; Hersam, M. C. Gate-tunable memristive phenomena mediated by grain boundaries in single-layer MoS_2 . *Nat. Nanotechnol.* **2015**, *10*, 403–406.
- (4) Santosh, K. C.; Longo, R. C.; Wallace, R. M.; Cho, K. Surface oxidation energetics and kinetics on MoS_2 monolayer. *J. Appl. Phys.* **2015**, *117*, 135301.
- (5) Chow, P. K.; Jacobs-Gedrim, R. B.; Gao, J.; Lu, T.-M.; Yu, B.; Terrones, H.; Koratkar, N. Defect-Induced Photoluminescence in Monolayer Semiconducting Transition Metal Dichalcogenides. *ACS Nano* **2015**, *9*, 1520–1527.
- (6) Li, L.; Yu, Y.; Ye, G. J.; Ge, Q.; Ou, X.; Wu, H.; Feng, D.; Chen, X. H.; Zhang, Y. Black Phosphorus Field-Effect Transistors. *Nat. Nanotechnol.* **2014**, *9*, 372–377.
- (7) Favron, A.; Gaufrè, E.; Fossard, F.; Phaneuf-L'Heureux, A.-L.; Tang, N. Y.-W.; Lévesque, P. L.; Loiseau, A.; Leonelli, R.; Francoeur, S.; Martel, R. Photooxidation and Quantum Confinement Effects in Exfoliated Black Phosphorus. *Nat. Mater.* **2015**, *14*, 826–832.
- (8) Liang, L.; Wang, J.; Lin, W.; Sumpter, B. G.; Meunier, V.; Pan, M. Electronic Bandgap and Edge Reconstruction in Phosphorene Materials. *Nano Lett.* **2014**, *14*, 6400–6406.

- (9) Li, Y.; Zhou, Z.; Zhang, S.; Chen, Z. MoS₂ Nanoribbons: High Stability and Unusual Electronic and Magnetic Properties. *J. Am. Chem. Soc.* **2008**, *130*, 16739–16744.
- (10) Lee, G.; Cui, X.; Kim, D.; Arefe, G.; Zhang, X.; Lee, C.; Ye, F.; Kenji, W.; Taniguchi, T.; Kim, P.; Hone, J. Highly Stable, Dual-Gated MoS₂ Transistors Encapsulated by Hexagonal Boron Nitride with Gate-Controllable. *ACS Nano* **2015**, *9*, 7019–7026.
- (11) Robertson, A. W.; Bhaskaran, H.; Warner, J. H. Controlled Preferential Oxidation of Grain Boundaries in Monolayer Tungsten Disulfide for Direct Optical Imaging. *ACS Nano* **2015**, *9*, 3695–3703.
- (12) Ly, T. H.; Chiu, M.-H.; Li, M.-Y.; Zhao, J.; Perello, D. J.; Cichocka, M. O.; Oh, H. M.; Chae, S. H.; Jeong, H. Y.; Yao, F.; Li, L.-J.; Lee, Y. H. Observing Grain Boundaries in CVD-Grown Monolayer Transition Metal Dichalcogenides. *ACS Nano* **2014**, *8*, 11401–11408.
- (13) Zhang, Y.; Zhang, Y.; Ji, Q.; Ju, J.; Yuan, H.; Shi, J.; Gao, T.; Ma, D.; Liu, M.; Chen, Y.; Song, X.; Hwang, H. Y.; Cui, Y.; Liu, Z. Controlled Growth of High-Quality Monolayer WS₂ Layers on Sapphire and Imaging its Grain Boundary. *ACS Nano* **2013**, *7*, 8963–8971.
- (14) Gao, J.; Chow, P. K.; Thomas, A. V.; Lu, T.-M.; Borca-Tasciuc, T.; Koratkar, N. Reduced Stability of Copper Interconnects due to Wrinkles and Steps on Hexagonal Boron Nitride Substrates. *Appl. Phys. Lett.* **2014**, *105*, 123108.
- (15) Kim, K. K.; Hsu, A.; Jia, X.; Kim, S. M.; Shi, Y.; Hofmann, M.; Nezich, D.; Rodriguez-Nieva, J. F.; Dresselhaus, M.; Palacios, T.; Kong, J. Synthesis of Monolayer Hexagonal Boron Nitride on Cu Foil Using Chemical Vapor Deposition. *Nano Lett.* **2012**, *12*, 161–166.
- (16) Wood, J. D.; Wells, S. a.; Jariwala, D.; Chen, K.; Cho, E.; Sangwan, V. K.; Liu, X.; Lauhon, L. J.; Marks, T. J.; Hersam, M. C. Effective Passivation of Exfoliated Black Phosphorus Transistors Against Ambient Degradation. *Nano Lett.* **2014**, *14*, 6964–6970.
- (17) Chamlagain, B.; Li, Q.; Ghimire, N. J.; Chuang, H. J.; Perera, M. M.; Tu, H.; Xu, Y.; Pan, M.; Xiao, D.; Yan, J.; Mandrus, D.; Zhou, Z. Mobility Improvement and Temperature Dependence in MoSe₂ Field-Effect Transistors on Parylene-C Substrate. *ACS Nano* **2014**, *8*, 5079–5088.
- (18) Cieslik, M.; Engvall, K.; Pan, J.; Kotarba, A. Silane-Parylene Coating for Improving Corrosion Resistance of Stainless Steel 316L Implant Material. *Corros. Sci.* **2011**, *53*, 296–301.
- (19) Mak, K. F.; McGill, K. L.; Park, J.; McEuen, P. L. The Valley Hall Effect in MoS₂ Transistors. *Science* **2014**, *344*, 1489–1492.
- (20) Mouris, S.; Miyachi, Y.; Matsuda, K. Tunable Photoluminescence of Monolayer MoS₂ via Chemical Doping. *Nano Lett.* **2013**, *13*, 5944–5948.
- (21) Mak, K. F.; He, K.; Lee, C.; Lee, G. H.; Hone, J.; Heinz, T. F.; Shan, J. Tightly Bound Trions in Monolayer MoS₂. *Nat. Mater.* **2012**, *12*, 207–211.
- (22) Chernikov, A.; Berkelbach, T. C.; Hill, H. M.; Rigos, A.; Li, Y.; Aslan, O. B.; Reichman, D. R.; Hybertsen, M. S.; Heinz, T. F. Exciton Binding Energy and Nonhydrogenic Rydberg Series in Monolayer WS₂. *Phys. Rev. Lett.* **2014**, *113*, 076802.
- (23) Eksik, O.; Gao, J.; Shojaee, S. A.; Thomas, A.; Chow, P.; Bartolucci, S. F.; Lucca, D.; Koratkar, N. Epoxy Nanocomposites with Two-Dimensional Transition Metal Dichalcogenide Additives. *ACS Nano* **2014**, *8*, 5282–5289.
- (24) Ross, J. S.; Wu, S.; Yu, H.; Ghimire, N. J.; Jones, A. M.; Aivazian, G.; Yan, J.; Mandrus, D. G.; Xiao, D.; Yao, W.; Xu, X. Electrical Control of Neutral and Charged Excitons in a Monolayer Semiconductor. *Nat. Commun.* **2013**, *4*, 1474.
- (25) Lopez-Sanchez, O.; Lembke, D.; Kayci, M.; Radenovic, A.; Kis, A. Ultrasensitive Photodetectors Based on Monolayer MoS₂. *Nat. Nanotechnol.* **2013**, *8*, 497–501.
- (26) Splendiani, A.; Sun, L.; Zhang, Y.; Li, T.; Kim, J.; Chim, C. Y.; Galli, G.; Wang, F. Emerging Photoluminescence in Monolayer MoS₂. *Nano Lett.* **2010**, *10*, 1271–1275.
- (27) Mak, K. F.; Lee, C.; Hone, J.; Shan, J.; Heinz, T. F. Atomically Thin MoS₂: A New Direct-Gap Semiconductor. *Phys. Rev. Lett.* **2010**, *105*, 136805.
- (28) Mak, K. F.; He, K.; Shan, J.; Heinz, T. F. Control of Valley Polarization in Monolayer MoS₂ by Optical Helicity. *Nat. Nanotechnol.* **2012**, *7*, 494–498.
- (29) Salvatl, L.; Makovsky, L. E.; Stencel, J. M.; Brownls, F. R.; Hercules, D. M. Surface Spectroscopic Study of Tungsten-Alumina Catalysts Using X-Ray Photoelectron, Ion Scattering, and Raman Spectroscopies. *J. Phys. Chem.* **1981**, *104*, 3700–3707.
- (30) Nirupama, V.; Sekhar, M. C.; Subramanyam, T. K.; Uthanna, S. Structural and Electrical Characterization of Magnetron Sputtered MoO₃ Thin Films. *J. Phys. Conf. Ser.* **2010**, *208*, 012101.
- (31) Reddy, B. M.; Chowdhury, B.; Reddy, E. P.; Fernández, A. An XPS Study of Dispersion and Chemical State of MoO₃ on Al₂O₃-TiO₂ Binary Oxide Support. *Appl. Catal., A* **2001**, *213*, 279–288.
- (32) Chow, P. K.; Singh, E.; Viana, B. C.; Gao, J.; Luo, J.; Li, J.; Lin, Z.; Elías, A. L.; Shi, Y.; Wang, Z.; Terrones, M.; Koratkar, N. Wetting of Mono and Few-Layered WS₂ and MoS₂ Films Supported on Si/SiO₂ Substrates. *ACS Nano* **2015**, *9*, 3023–3031.
- (33) Kozbial, A.; Gong, X.; Liu, H.; Li, L. Understanding the Intrinsic Water Wettability of Molybdenum Disulfide (MoS₂). *Langmuir* **2015**, *31*, 8429–8435.
- (34) Addou, R.; McDonnell, S.; Barrera, D.; Guo, Z.; Azcat, A.; Wang, J.; Zhu, H.; Hinkle, C. L.; Quevedo-Lopez, M.; Alshareef, H. N.; Colombo, L.; Hsu, J. W. P.; Wallace, R. M. Impurities and Electronic Property Variations of Natural MoS₂ Crystal Surfaces. *ACS Nano* **2015**, *9*, 9124–9133.
- (35) Addou, R.; Colombo, L.; Wallace, R. M. Surface Defects on Natural MoS₂. *ACS Appl. Mater. Interfaces* **2015**, *7*, 11921–11929.
- (36) N'Diaye, M.; Pasquarelli-Grizon, F.; Massin, P.; Baslé, M. F.; Chappard, D. Water Absorption of Poly(methyl Methacrylate) Measured by Vertical Interference Microscopy. *Langmuir* **2012**, *28*, 11609–11614.
- (37) Spivack, M. A.; Ferrante, G. Determination of the Water Vapor Permeability and Continuity of Ultrathin Parylene Membranes. *J. Electrochem. Soc.* **1969**, *116*, 1592.